ISBN: 978-3-95450-248-6 ISSN: 2673-5490 doi: 10.18429/JACoW-IPAC2025-MOPB061

EXPERIMENTAL STUDY ON SOFT X-RAY GENERATION VIA INVERSE COMPTON SCATTERING AT CERN

V. Mușat*[1,2], P. N. Burrows[2], M. M. Calderon[1], S. Doebert[1], E. Granados[1], M. Hibberd[3], A. Latina[1]
[1] CERN, Geneva, Switzerland
[2] John Adams Institute, University of Oxford, Oxford, UK
[3] University of Manchester, Manchester, UK

Abstract

This study explores the feasibility of using Compton Backscattering (CBS) as a compact source for generating photons in the extreme ultraviolet (EUV) to soft X-ray range, with potential applications in biological imaging and modern lithography. A CBS experiment was conducted at the AWAKE Run 2c test injector (ARTI), where electron bunches, accelerated up to 6 MeV by a high-gradient, brazing-free S-band photogun were collided with 1030 nm infrared pulses from the PHAROS femtosecond laser. The electron and laser beamlines were optimised for maximum CBS photon flux.

INTRODUCTION

Water window X-rays are critical for the 2D and 3D imaging of cellular wet samples [1]. Characterized by photon wavelengths ranging from 2.33 nm to 4.40 nm, and transparent to water, these X-rays have been primarily used for experiments in large-scale photon sources [2]. Emerging technology and increased demand have driven the development of table-top water window X-ray sources [3] as a cost-effective alternative to FEL or synchrotron experiments. At a longer wavelength of 13.5 nm, extreme ultraviolet (EUV) lithography is used for state-of-the-art chip production [4]. In order to obtain even smaller microchips, research has been directed towards developing light sources reaching beyond the EUV, towards 6.7 nm wavelength [5, 6].

This paper considers the potential of Compton backscattering (CBS) to drive compact soft X-ray light sources. Narrow-bandwidth CBS photons are generated from the interaction of a high-energy electron bunch with a high-intensity laser pulse, as described by the Thomson and Klein-Nishina cross sections [7]. The energy tunability and small footprint of linac-based CBS sources further benefit from developments in high gradient acceleration and high repetition rate injection technology developed for the Compact Linear Collider (CLIC) and CompactLight (XLS) [8]. The electron gun of the AWAKE Run2 Test Injector (ARTI) in the CLIC Test Facility 2 (CTF2) was used as a demonstrator for soft X-ray generation via Compton backscattering.

ACCELERATOR BASELINE

A schematic of the current set-up is shown in Fig. 1. The S-band electron gun was fabricated using brazing-free technology [9]. It reaches a maximum RF gradient of 120 MV/m, accelerating electron bunches up to 6 MeV. The nominal accelerating gradient is 106.7 MV/m, which was used to reach an electron beam energy of 5.5 MeV, and a relative energy spread of 0.2%. The electron source consists of a copper cathode, releasing electrons with a small thermal emittance under a moderate vacuum level of 6×10^{-8} mbar. A PHAROS laser is used to generate the electron bunches, emitting 2 mJ infrared pulses with a repetition rate of 10 Hz. To match the copper work function and ensure a small thermal emittance, the laser passes through two second harmonic generation (SHG) stages to reach a wavelength of 257 nm. An optical telescope is used to focus the laser on the cathode. Up to 440 µJ of UV light were obtained for a laser pulse length of 265.5 fs FWHM. For a stretched pulse length of 775.7 fs FWHM, the energy on the cathode decreased to 50 µJ. A maximum bunch charge of 800 pC was measured with the smallest laser pulse length of 265.5 fs FWHM and a $1/e^2$ waist size of 540 µm. A summary of the electron and laser beam parameters at the interaction point (IP) is provided in Table 1 [10].

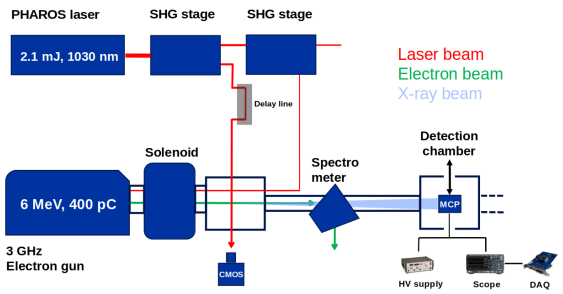

Figure 1: Schematic diagram of the AWAKE Run2 Test Injector set-up for the Compton backscattering experiment.

Beam Transport and Diagnostics

The position and beam size of the laser on the cathode was tracked using a virtual cathode camera set-up [11, 12]. Following the acceleration of the electron bunch, a focusing solenoid located 0.25 m from the cathode was used to focus the electron beam. Retractable OTR and YAG:Ce screens at 0.57 m were used to obtain an electron beam profile on a CMOS camera, as shown in Fig. 2. This location was used as the interaction point for the CBS experiment. Beam energy measurements were taken using a dipole spectrometer. At the end of the beamline, a Faraday cup was used for bunch charge measurements. The bunch charge stability was around 5%.

* vlad.musat@cern.ch

ISBN: 978-3-95450-248-6 ISSN: 2673-5490 doi: 10.18429/JACoW-IPAC2025-MOPB061

Table 1: Parameters of the Electron, Laser, and X-ray Beam at the Interaction Point

Parameter	Value
Beam energy [MeV]	5.5
Electron RMS spot size [μm]	100
Bunch charge [pC]	210
RMS bunch length [ps]	2
Crossing angle [°]	90
Laser RMS spot [μm]	25
Pulse energy [mJ]	1
RMS pulse length [ps]	0.9
Laser wavelength [nm]	1030
Photon energy [eV]	255
Collection angle [mrad]	21.4
Detected photons [RFT]	21
Generated photons [RFT]	2.6×10^3

The IR laser leakage from the first SHG stage was used to induce Compton backscattering at the IP. A 90° collision angle enabled the laser to be visualised on the same camera system as the electron beam. The laser was focused to a 25 μm spot at the IP.

ELECTRON BEAM OPTIMISATION

In order to maximise the generated photon flux, the electron beam was optimised for a small transverse and longitudinal emittance at the interaction point. To achieve this, the position of the UV laser on the cathode and the solenoid were aligned with respect to the gun electric field axis. Additionally, the optimal RF phase and laser spot size were obtained from parametric scans of the solenoid strength while looking at the electron beam size at the IP. A detailed account of the beamline optimisation is presented in Ref. [10].

The laser-cathode alignment was obtained by RF focusing the electron beam on the YAG screen. This was achieved by locating the laser position that minimizes the variation in electron beam position as a function of RF phase. The solenoid was aligned by moving its position to minimize the variation in electron beam position as a function of the solenoid strength. Together, the solenoid and laser-cathode alignments led to a 40% decrease in the minimal electron spot size obtained.

Simulations of the electron beamline performed with RF-Track [13] indicate that the beam emittance can be further reduced by tuning the RF phase and the laser spot size. Experimental parametric scans of the electron beam size at the IP against the solenoid strength confirm an optimal value for the RF phase of −10°. For the laser spot size on the cathode, an X/Y value of 201/268 μm was chosen.

X-RAY DETECTION CHAMBER

The choice of X-ray detector depended on several factors. First, given the small number of detectable X-ray photons, a high detection efficiency is required, along with a suitably large active area due to the wide photon emission angle. Additionally, the detector requires a gain mechanism allowing for the amplification of a small input signal. Due to the high absorption rate of soft X-rays in air, the detector also has to be vacuum-compatible.

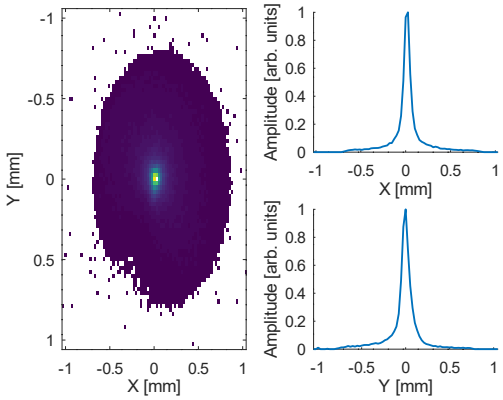

Figure 2: The measured profile of the electron beam at the IP following the beamline optimisation.

Due to the large emission angle of the X-rays, the detector must be placed as close as possible to the IP. The detection chamber was therefore installed a few centimeters after the spectrometer dipole. In order to allow for charge measurements with the Faraday cup at the end of the beamline, the detector had to be light enough to be movable with a linear drive. Given all the requirements, a microchannel plate (Hamamatsu F9890-13) was chosen. A schematic of the detection chamber is shown in Fig. 3.

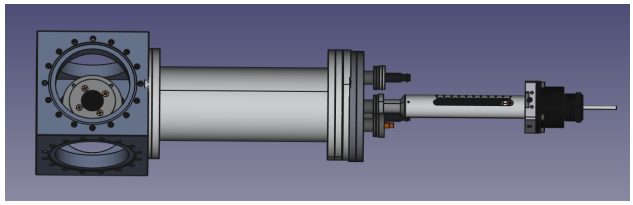

Figure 3: Schematic of the X-ray detection chamber. The MCP is housed in a cubical vacuum chamber. A custom flange is used to connect the detector to a power source, oscilloscope, and linear drive.

X-ray Detection Chamber Set-up

To allow for the in-vacuum operation of the microchannel plate, a detection chamber was designed. The cubical chamber was connected through a vacuum pipe to a feedthrough flange. The flange included two high-voltage vacuum feedthroughs to power the detector, one SMA feedthrough to transmit the signal from the MCP, and a linear drive. The latter was used to move the detector along the vertical axis and clear the beam path for the Faraday cup placed at the end of the beamline.

ISBN: 978-3-95450-248-6 ISSN: 2673-5490 doi: 10.18429/JACoW-IPAC2025-MOPB061

Detector Calibration

The MCP detector was calibrated using an Fe-55 radioactive x-ray source. A gain calibration was done, which allows the estimation of the number of photons recorded for a given applied voltage to the detector. The results, shown in Fig. 4, indicate an exponential response of the signal area and peak-to-peak to changes with respect to the MCP supply voltage. A typical MCP signal response from a single photon event is shown in Fig. 4.

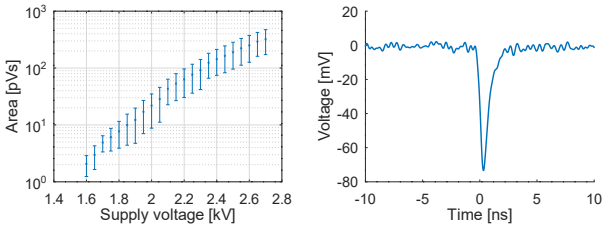

Figure 4: Gain curve (left) and typical signal response (right) from the MCP calibration with an Fe-55 source.

RF-TRACK SIMULATIONS

The measured electron and laser beam parameters at the IP from Table 1 were used as an input for the RF-Track CBS module in order to estimate the flux performance. The flux was significantly reduced due to the use of a 90° crossing angle and a low energy electron beam. Since the CBS photon emission angle is inversely proportional to the electron beam energy, 93% of the CBS does not reach the MCP active area and is instead absorbed by the beam pipe. A total of 200 photons were predicted to reach the detector per bunch crossing. Given the 12% detection efficiency of the MCP, 21 photons would then be detected [14]. A peak photon energy of 255 eV was derived from simulations.

SPATIAL AND TEMPORAL ALIGNMENT

Given the small spot sizes involved in the interaction, the spatial alignment needs to be precise within tens of micrometers, along with a temporal alignment of a few picoseconds.

Spatial Alignment

The spatial alignment was first achieved by aligning the electron and laser through a 0.85 mm diameter hole in the OTR screen. Due to the 45° tilt of the OTR screen, the horizontal diameter is projected to 0.60 mm. To avoid spikes in vacuum, holes in the OTR screen were made using a laser cutter before installation. The position of the electron beam was scanned around the hole, and the total light intensity collected by the camera recorded, as shown in Fig. 5. The electron beam was aligned by centering it at the point of minimum light intensity. Similarly, the IR laser was spatially aligned by finding its center point in the OTR hole, which corresponds to the region of maximum light intensity, since the laser needed to pass through the OTR hole to reach the camera. Given the milimeter diameter of the OTR hole, and small IP laser spot size, the centering of the two beams was challenging. To ease the process, the silicon wafer-based OTR screen was replaced with a high purity 0.025 mm thick Aluminium foil. The IR laser was used to make a hole in the foil, and the electron beam was focused through the created hole, which spanned a few tens of micrometers.

Temporal Alignment

A preliminary temporal alignment was achieved by using the UV laser reflected from the copper cathode. Since the electron beam path is similar to the reflected UV beam path, the latter can be used to set up a purely optical pre-alignment. The path length of the UV laser was matched to the IR laser under a Michelson interferometer-like setup. Both laser beams were detected and aligned temporally using an ultrafast photodiode. This was used to calibrate the step size of the optical delay stage and limit the delay scan range to 40 ps, which corresponds to the photodiode rise time. Delay scans typically have a step size of 0.5 ps.

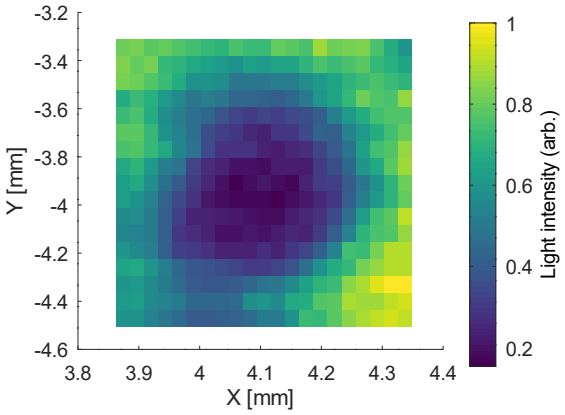

Figure 5: Two-dimensional scan of the electron position around the interaction region, colorgraded by the total light intensity collected by the CMOS camera.

CONCLUSIONS AND OUTLOOK

The 1 m distance from the electron source to the MCP detector makes the ARTI injector one of the most compact RF-based CBS sources in the literature. The electron beamline was optimised to provide the maximum possible flux. Simulations in RF-Track were used to optimise the beamline and predict the scattered photon flux. An Fe-55 radioactive source was used to calibrate the MCP. The spatial alignment between the laser and electron beam was obtained by centering the two beams through a hole in the OTR imaging screen. The temporal alignment was preliminarily performed using the cathode-reflected UV laser beam, and the interaction IR beam. Scans of the optical delay stage have been performed in order to locate the X-ray signal. Recently, a signal consistent with CBS has been detected. A comprehensive study is currently underway, aiming for a detailed characterisation of the scattered X-ray beam and benchmarking of RF-Track's CBS module against measurements at ARTI.

ISBN: 978-3-95450-248-6 ISSN: 2673-5490 doi: 10.18429/JACoW-IPAC2025-MOPB061

REFERENCES

[1] G. D. Stasio *et al.*, "Feasibility tests of transmission x-ray photoelectron emission microscopy of wet samples", *Rev. Sci. Instrum.*, vol. 71, no. 1, pp. 10–14, 2000. doi:10.1063/1.1150151

[2] S. Schreiber, "First lasing in the water window with 4.1 nm at FLASH", in *Proc. FEL'11*, Shanghai, China, Aug. 2011, pp. 164–165. https://jacow.org/FEL2011/papers/TUOBI2.pdf

[3] M. Kördel *et al.*, "Laboratory water-window x-ray microscopy", *Optica*, vol. 7, no. 6, pp. 620–627, 2020. doi:10.1364/OPTICA.393014

[4] T. Manouras and P. Argitis, "High sensitivity resists for EUV lithography: A review of material design strategies and performance results", *Nanomaterials*, vol. 10, no. 8, p. 1593, 2020. doi:10.3390/nano10081593

[5] N. Mojarad, J. Gobrecht, and Y. Ekinci, "Beyond EUV lithography: A comparative study of efficient photoresists' performance", *Sci. Rep.*, vol. 5, p. 9235, 2015. doi:10.1038/srep09235

[6] D. F. Ratner and A. W. Chao, "Steady-state microbunching in a storage ring for generating coherent radiation", *Phys. Rev. Lett.*, vol. 105, no. 15, p. 154 801, 2010. doi:10.1103/PhysRevLett.105.154801

[7] O. Klein and T. Nishina, "Über die Streuung von Strahlung durch freie Elektronen nach der neuen relativistischen Quantendynamik von Dirac", *Z. Phys.*, vol. 52, no. 11–12, pp. 853–868, 1929. doi:10.1007/BF01366453

[8] G. D'Auria *et al.*, "The CompactLight design study", *Eur. Phys. J. Spec. Top.*, vol. 233, no. 1, pp. 1–208, 2024. doi:10.1140/epjs/s11734-023-01076-0

[9] D. Alesini *et al.*, "Design, realization, and high power test of high gradient, high repetition rate brazing-free S-band photogun", *Phys. Rev. Accel. Beams*, vol. 21, no. 11, p. 112 001, 2018. doi:10.1103/PhysRevAccelBeams.21.112001

[10] V. Musat *et al.*, "Status of the commissioning of the X-band injector prototype for AWAKE Run 2c", in *Proc. IPAC'24*, Nashville, TN, USA, pp. 121–124, 2024. doi:10.18429/JACoW-IPAC2024-MOPC28

[11] E. Panofski, A. Jankowiak, T. Kamps, and G. Klemz, "Virtual cathode drive laser diagnostics with a large dynamic range for a continuous wave SRF photoinjector", in *Proc. IPAC'14*, Dresden, Germany, Jun. 2014, pp. 2251–2253, 2014. doi:10.18429/JACoW-IPAC2014-WEPME001

[12] R. Akre *et al.*, "Commissioning the Linac Coherent Light Source injector", *Phys. Rev. ST Accel. Beams*, vol. 11, no. 3, p. 030 703, 2008. doi:10.1103/PhysRevSTAB.11.030703

[13] A. Latina, *RF-Track Reference Manual Version 2.1.6*, 2016. doi:10.5281/zenodo.3887084

[14] W. Parkes, R. Gott, and K. A. Pounds, "Soft x-ray studies of channel multipliers and multiplier arrays", *IEEE Trans. Nucl. Sci.*, vol. 17, no. 3, pp. 377–384, 1970. doi:10.1109/TNS.1970.4325713